Chiral Metal–Organic Nanotubes

DOI: 10.1002/anie.201004921

A Porous Flexible Homochiral $SrSi_2$ Array of Single-Stranded Helical Nanotubes Exhibiting Single-Crystal-to-Single-Crystal Oxidation Transformation**

*You-Gui Huang, Bin Mu, Paul M. Schoenecker, Cantwell G. Carson, Jagadeswara R. Karra, Yang Cai, and Krista S. Walton**

Since the first discovery of carbon nanotubes (CNTs) by Iijima in 1991,[1] the synthesis of hollow tubular structures from inorganic (e.g. C, B, N, Si)[2] and organic (e.g, cyclic oligomers)[3–5] building blocks has been intensely studied due to the potential applications in ion exchange, molecular sieves, catalysis, molecular devices, and sensors. In recent years, an increasing demand from pharmaceutical and biochemical industries for production of enantiopure species has stimulated much interest in developing these materials for chiral separations. Carbon nanotubes possess chirality due to the helical twist of graphitic sheets about the tube axis[6] but cannot be applied as enantiospecific adsorbents without the incorporation of functional groups onto the surface.[7] Organic nanotubes are more easily functionalized than CNTs but suffer from limited tube diameters (1–2 nm) and polydisperse assemblies.[8]

Employing metal–organic helices as building blocks to hierarchically assemble helical nanotubes is a conceivable strategy for synthesizing functionalized structures with enantioselective features.[9,10] These chiral nanotubes can form by an interweaving[11,12] or parallel association[13,14] of single- and multi-stranded helices. Quintuple helices have been used by Lin et al. to form an array of interlocked chiral nanotubes with 20 Å openings.[13] A parallel association of octuple helices has been shown by Wang et al. to form a 3D chiral network of nanotubes with openings of 19.4 Å by 22.4 Å.[14] Chiral nanotubes with negligible porosity (< 2 Å inner diameter) formed by quadruple-stranded helices were recently reported by Vaquerio et al.[15] In contrast to these examples, a *single* helix spiraling with a short pitch (width of one complete helix turn) can form hollow tubular structures with uniform, fixed internal diameters. Two exceptional examples of single-stranded helical metal–organic nanotubes have been presented in the literature: a dense homochiral array of nanotubes originating from nine-fold interlocking helices,[16] and a chiral nanotube formed from the helical assembly of alternating *p*-sulfonatocalix[4]arenas and lanthanide ions. The latter, reported by Atwood et al.,[17] presents the rare discrete helical metal–organic nanotube. The development of chiral metal–organic nanotubes is still in its infancy, and most of them are constructed from interweaving helices, which usually result in an achiral framework because of the alternating array of opposite-handed nanotubes.[16]

Herein, we report the synthesis of a homochiral array[18] of metal–organic nanotubes constructed from achiral sources and possessing three novel features: 1) nanotubular channels formed by a single-stranded helix with no interlocking, interweaving, or parallel association; 2) large, hollow, right-handed nanotubes of 1.4 nm inside diameter; 3) oxidation induced single-crystal-to-single-crystal transformation. So far, most of the dynamic behaviors of metal–organic frameworks (MOFs) (e.g., gate opening) depend on guest molecule adsorption/desorption.[18–20] However, single-crystal-to-single-crystal transformations involving oxidation are rare. Redox-active frameworks have shown their utility as reducing agents in preparing relatively monodispersed small metal nanoparticles.[21,22] In this work, the redox-active porous homochiral **srs** framework $[\{Cu_{12}^{I}(trz)_8\}\cdot 4Cl\cdot 8H_2O]_n$ (**1a**) (Htrz = 1,2,4-triazole) consists of single-stranded helix spiraling nanotubes, which can be oxidized under atmospheric conditions forming the topologically equivalent $[\{Cu_{12}^{II}(trz)_8\}\cdot 4Cl\cdot 12(OH)\cdot 2(H_2O)]_n$ (**1b**), accompanied by an expansion in the cell volume of 12.51%.

Colorless or pale-colored crystals of **1a** were obtained from the in situ reaction of $CuCl_2\cdot(H_2O)_2$ and 3-amino-5-carboxylic-1,2,4-triazole under hydrothermal conditions. It is noteworthy that the Cu^{II} ions were reduced to Cu^{I} ions during the reaction, which was revealed by the yellow product and supported by X-ray photoelectron spectroscopy (XPS). The ligand 3-amino-5-carboxylic-1,2,4-triazole was originally chosen for its multiple Lewis basic sites (the carboxylic acid group, the amino group, and the three imino nitrogen atoms) with the intention of forming porous metal–organic frameworks with functional groups. Unexpectedly, the ligand underwent decarboxylation and deamination to produce 1,2,4-triazole.

Single-crystal X-ray crystallography reveals that compound **1a** is an infinite 3D framework, crystallizing in the chiral tetragonal space group $I4_122$.[23] The asymmetric unit

[*] Dr. Y.-G. Huang, B. Mu, P. M. Schoenecker, Dr. C. G. Carson, J. R. Karra, Y. Cai, Prof. K. S. Walton
School of Chemical & Biomolecular Engineering
Georgia Institute of Technology
311 Ferst Dr. NW, Atlanta, GA 30332 (USA)
Fax: (+1) 404-894-2826
E-mail: krista.walton@chbe.gatech.edu

[**] We are grateful for financial support from the Department of Defense under awards W911NF-10-1-0076 and PECASE W911NF-10-1-0079 and the National Science Foundation (CBET 1009682 and CAREER award CBET 0969261). We thank Prof. L. D. Williams and Dr. E. Aaron for the measurement of UV and CD spectra, and thank Prof. W. Henderson for the measurement of XPS.

Supporting information for this article is available on the WWW under http://dx.doi.org/10.1002/anie.201004921.

contains half and one-fourth of two crystallographically independent Cu^{I} ions and half of a trz anion. Other disordered anions and guest molecules are not crystallographically well-defined. To achieve charge neutrality, there is one-fourth of Cl^{-} ion in each asymmetric unit as supported by the observation of Cl2p peak at 198.1 eV in XPS (Supporting Information, Figures S7, S8). Cu1 is coordinated by two N atoms with a N-Cu1-N angle of 160.75° and Cu1–N bond length of 1.811 Å, while Cu2 is coordinated by two N atoms in linear geometry with a Cu2–N bond length of 1.890 Å (Figure S11). The trz ligands adopt μ_3 bridging mode to connect to three Cu^{I} ions.

The complicated framework of compound **1a** can be described as an array of Cu^{I}-linked single-stranded helical nanotubes. The Cu1 ions are bridged by the N1,2 atoms of trz ligands to form an infinite left-handed helical chain running along the *c*-axis (Figure 1a). The helix is generated around

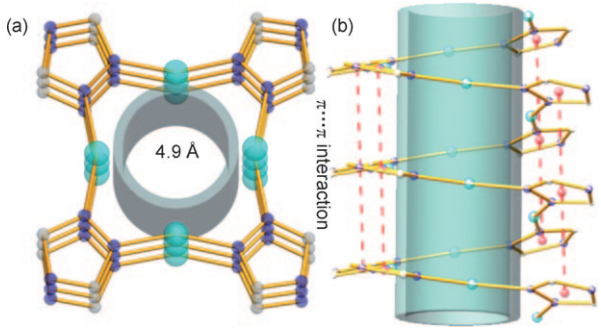

Figure 1. a) Top view of the small left-handed single-stranded helix nanotube in compound **1a**. b) Side view of the helical nanotube showing π···π interactions.

the crystallographic 4_1 screw axis. Remarkably, the single-stranded helical species spirals with a very short pitch and the bulk of the trz component is pointing away from the 4_1 screw axis to give rise to a gyroid nanotube. The single-stranded helical nanotube is stabilized by strong π···π interactions among trz ligands from adjacent pitches, i.e., parallel stacking with face to face separation of 3.224 Å (Figure 1b). The fragment that determines the pitch of the helix is composed of four Cu1 ions and four trz ligands bridged alternately (see Figure 3d). The pitch length of 3.224 Å is identical to the *c*-axis length. The cross-section of the helical nanotube is formed by Cu1-N2-N2-Cu1 structural motif with an exterior wall diameter of around 7.4 Å. The interior channel diameter or pore opening is approximately 4.9 Å.

As mentioned above, the trz ligands have an affinity for μ_3-coordination mode, two of which are occupied by two Cu1 ions in the above single-stranded helical nanotube, therefore the remaining N4 atom provides an additional binding site to assemble the small single-stranded helical nanotube into a 3D array. Each nanotube serves as a secondary building unit and is further linked to its four adjacent neighbors in two orthogonal directions through Cu2 ions generating a 3D homochiral framework (Figure S12). The most intriguing feature in this 3D framework is the giant hollow helical nanotube formed by the four adjacent left-handed nanotubes (Figure 2d). The large nanotubes run along the *c*-axis with the same pitch length as the small nanotubes (3.224 Å), but have opposite handedness (Figure 2b). The giant helical nanotube

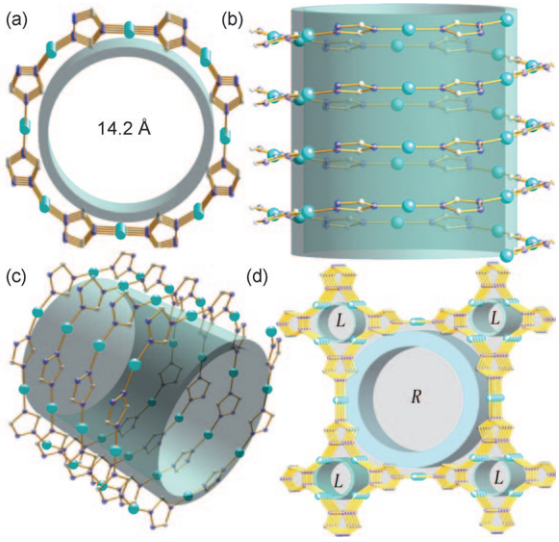

Figure 2. a) Top view of the giant right-handed single-stranded helix nanotube with 8-Cu/trz pitches. b) Side view of the giant helical nanotube. c) Perspective view of the giant helical nanotube. d) The giant hollow right handed helical nanotube formed by Cu2-linked four small single-stranded helix nanotubes.

is stabilized by strong π···π interactions among trz ligands from adjacent pitches. In contrast to the 4 Cu^{I}/trz helical fragment pitch, the fragment determining a pitch in this giant nanotube is composed of eight Cu^{I} ions and eight trz ligands bridged alternately (Figure 3c), resulting in a much larger

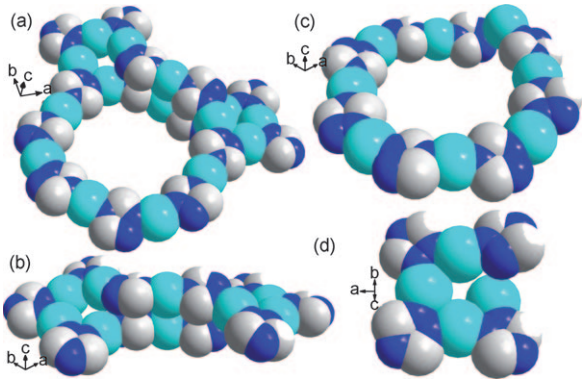

Figure 3. a) The big cavity defined by three 10-membered rings of 10 Cu/trz. b) The twisted 10-membered ring isolating adjacent channels in the framework. c) The 8-Cu/trz helical pitch of the giant single-stranded helix nanotube. d) The 4-Cu/trz helical pitch of the small single-stranded helix nanotube.

scale with an exterior wall diameter of around 16.5 Å, and an interior tubular diameter of around 14.2 Å (Figure 2a,c). The cross-section of this nanotube is formed by N2-Cu1-N2 structural motif (Figure 2a).

In the view of topology, by treating trz ligands as nodes and Cu ions as linkers, the 3D framework can be symbolized to be a 3-connected net, well known as the net of the Si atoms in the $SrSi_2$ structure, with symbol **srs** (Figure S13). This net is one of the five regular 3-periodic nets and is the only chiral one. The repeat unit of the **srs** net is composed of three 10-membered rings of 10 Cu^I/trz components, which define a big cavity (Figure 3a). Each big cavity communicates with its two adjacent cavities along the *c* axis through big windows of eight Cu^I/trz helical fragments (Figure 3c) to form the two types of 1D gyroidal channels along the *c* axis (Figure 2d). The small tubular channel is formed by a single-stranded helix with 4 Cu^I/trz pitches, while the large one is formed by a single-stranded helix with 8 Cu^I/trz pitches. The cavities between adjacent channels are isolated by the twisted 10-rings of 10 Cu^I/trz components (Figure 3b).

Prior to this work, hollow chiral nanotubular architectures have usually been formed either by interwoven helices[11,12] or by parallel aligned helices.[13,14] Also, it has been demonstrated that single-stranded helices with long pitches interlock easily with each other to form dense arrays.[24] Here, it is supposed that the unusually short helical pitch in **1a** effectively prevents interlocking and is a key factor in the formation of our large hollow single-stranded helical nanotube. We are aware of one exceptional case in which discrete metal–organic helical nanotubes are formed by assembly of alternating *p*-sulfonatocalix[4]arenas and lanthanide ions. However, the discrete nanotubes do not form the same type of ordered array as shown here, and the pore space of the nanotubes is closed due to disordered lanthanum ions and hydrated sodium ions.[17]

A solution of compound **1a** in CH_3CN with concentration of 5.85×10^{-6} M was prepared for UV absorption. The UV absorption spectrum exhibits two absorption bands around 225 nm and 309 nm which are attributed to π–π* and n–π* transitions, respectively. In order to better validate the chiral properties, six parallel CD measurements were performed on 5.85×10^{-6} M CH_3CN solution of compound **1a** from different batches. All give the same expected CD spectra. The results show negative Cotton effect in the region of both transitions, indicating the bulk sample of compound **1a** is enantioenriched (Figure 4).

Because there are no driving forces of symmetry breaking crystallization, such spontaneous asymmetrical crystallization presented here is unexpected. The origin of chirality of compound **1a** should be closely related to the chiral **srs** net, whose chirality arises from the 4_1 [100] and 3_1 [111] screw axes of the same handedness propagating in all crystallographically equivalent directions.[25] The asymmetrical crystallization of the bulk sample from achiral precursors without any enantiopure sources is an unusual phenomenon. Like other well-known examples (e.g., $NaClO_3$), the initial crystals generated by symmetry breaking may seed the handedness of the bulk product, and thus the particular handedness of the bulk formed.[26,27]

The color of compound **1a** changes from yellow to green after several weeks depending on the humidity (Figure S14), implying the oxidation of Cu^I in air is promoted by moisture generating a different phase $[\{Cu_{12}^{II}(trz)_8\}\cdot4Cl\cdot12(OH)\cdot2(H_2O)]_n$ (**1b**). The oxidation of Cu^I to Cu^{II} was confirmed by the XPS of both compound **1a** and **1b**. In the XPS spectrum of compound **1a**, the peak corresponding to the core-level Cu $2p_{3/2}$ XPS transition is observed at 934.1 eV, while that of compound **1b** is at 935.4 eV accompanied by a satellite peak towards a higher binding energy of 945.8 eV (Figure S9). The weak satellite feature observed in compound **1b** is characteristic of a compound having a d^9 configuration ground state.[28] The binding energy peak shift of 1.3 eV is consistent with the reported difference of binding energy peak between Cu_2O to CuO.[28]

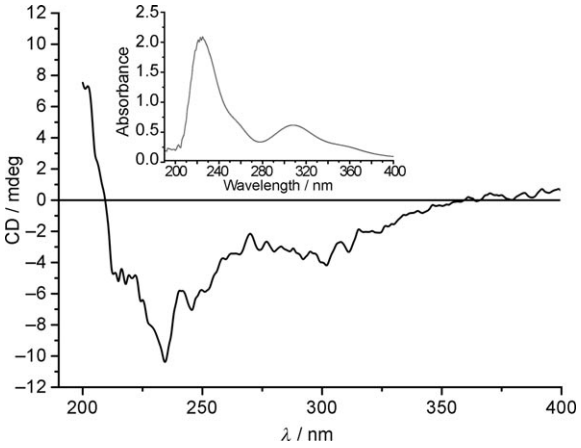

Figure 4. The CD spectrum of 5.85×10^{-6} M solution of compound **1a** in CH_3CN. Inset: UV absorption of 5.85×10^{-6} M solution of compound **1a** in CH_3CN

Remarkably, the crystal remained intact throughout this transformation, enabling the structure of compound **1b** to be determined. Single-crystal X-ray analysis revealed a new crystallographic form, wherein the framework connectivity and space group are maintained with unit cell parameters of $a=b=20.7391$, $c=3.3462$ Å, and $V=1439.23$ Å^3.[23] The transformation implies an increase of more than 0.82 Å of *a* and *b* axes and an increase of 0.12 Å of *c* axis, and is accompanied by an expansion in the cell volume of 12.51% (160.61 Å^3). The elongation of axes implies that the single-stranded helical nanotubes are enlarged, and the helical pitches are elongated. Indeed, for the smaller nanotube (with 4 Cu^I/trz pitch), the exterior wall diameter and the interior channel diameter expand to 7.6 and 5.1 Å, respectively; and those of the larger nanotube (with 8 Cu^I/trz pitch) expand to 17.1 and 14.8 Å respectively. This transformation was cross-checked by the shift to lower angles of XRD peaks of compound **1b** compared to those of compound **1a** (Figure 5 and Figures S1, S2). The peaks corresponding to [110], [220], [420] planes shift from 6.26° to 6.01°, 12.70° to 12.04°, and 20.10° to 19.10°, respectively.

Two mechanisms have been proposed to explain such breathing behavior.[29] The first is related to host–guest interactions and the second to the intrinsic flexibility of the framework itself, which is induced by the existence of weak points within the skeleton, allowing the deformation of the network under the action of a stimulus. Such a deformation of the framework structure is usually associated with the

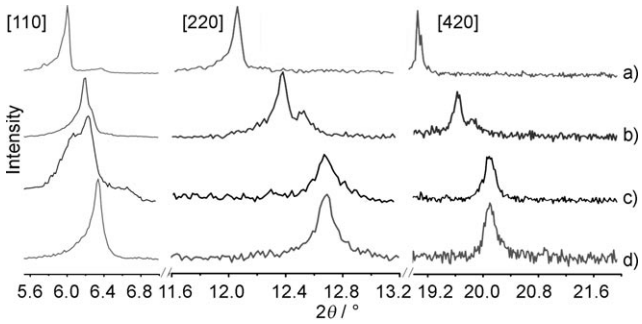

Figure 5. Shift of XRD peaks upon oxidation or dehydration. a) Compound **1b**, b) dehydrated **1b**, c) compound **1a**, d) dehydrated **1a**.

modifications of the bridging ligands[30] and/or metal coordination[31] sphere (e.g., solvent removal or elongation of bonds). The trz ligand in **1a** and **1b** is rigid and consequently is not responsible for the structural deformation. Instead, the expansion of the framework is most likely explained by the geometry changes of the coordination modes of Cu ions. Upon transformation, the Cu1–N2 and Cu2–N1 bonds are elongated from 1.811 to 1.935 and 1.890 to 2.013 Å, respectively; the N2-Cu1-N2A bond angle changes from 160.75° to 159.22°. In addition, the planes of two trz ligands coordinated to Cu1 ions rotate along the N1-Cu1-N1 axis with dihedral angle change from 32.1° to 28.2° (Figure 6). All of this results in the deformation of the whole 3D **srs** framework.

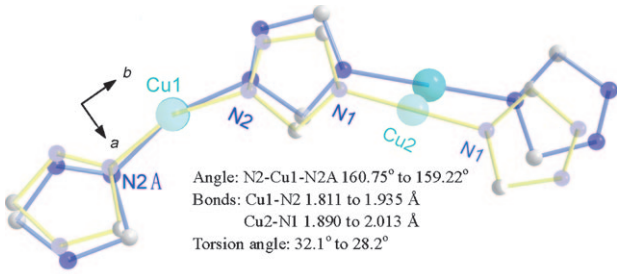

Figure 6. Comparison of the X-ray structures of **1a** (yellow) and **1b** (blue) with Cu1 positions superimposed.

As determined by PLATON,[32] there are two big cavities ($V = 270$ Å^3) and two small cavities ($V = 34$ Å^3) in each unit cell of compound **1a**, which locate in the large and small helical nanotubes, respectively. Therefore, the total void volume, V_{void} in compound **1a** is 47.5% per unit volume. However, part of the void is filled by disordered Cl^- ions which cannot be removed by activation. TGA performed on compound **1a** shows a weight loss of 8.98% (calcd 9.04%) from 30 to 180 °C (Figure S6), which corresponds to the loss of eight H_2O per formula unit. In compound **1b**, the big and small cavities expand to 351 and 40 Å^3, respectively, and the V_{void} is 54.3% per unit volume. Employing the squeeze option to determine the electron density in the unit cell of compound **1b**, the electron counts in cavities in each unit cell is 210 corresponding to four Cl^-, twelve OH^- ions and two H_2O molecules. The weight of 2.53% (calcd 2.13%) corresponding to two H_2O per formula unit is lost from 30 to 110 °C, as revealed by TGA (Figure S6). No further weight loss steps were observed below 280 °C for **1a** and 240 °C for **1b**, indicating the thermal stability of **1a** and **1b** up to 280 °C and 240 °C, respectively. Therefore the following reaction was proposed to take place during the oxidation transformation:

$$[\{Cu_{12}^{I}(trz)_8\}\cdot 4\,Cl\cdot 8\,H_2O]_n\ (\mathbf{1a}) + 3n\ O_2 \rightarrow [\{Cu_{12}^{II}(trz)_8\}\cdot 4\,Cl\cdot 12\,(OH)\cdot 2\,(H_2O)]_n\ (\mathbf{1b}).$$

After removal of the guest H_2O molecules, both dehydrated frameworks of **1a** and **1b** do not change their structures (except slightly shrinking) as revealed by XRD (Figure 5, Figures S4, S5). Despite the presence of counter anions, the permanent porosity of dehydrated **1a** was demonstrated by CO_2 adsorption isotherms at 298 K. The amount of CO_2 uptake at 1 bar (0.79 mmol g^{-1}) is comparable to that of IRMOF-1[33] (Figure S10).

In conclusion, we have prepared a porous flexible homochiral **srs** framework of single-stranded helical nanotubes. The enantiomeric nature of the bulk material was confirmed by circular dichroism (CD) spectra. The Cu^I ions in the framework can be oxidized to Cu^{II} under atmospheric conditions through single-crystal-to-single-crystal transformation forming a different, but topologically equivalent, phase. The transformation is accompanied by an expansion in the cell volume of 12.51%. Our results highlight an important topic and provide vision for the development of chiral helical metal–organic nanotube-based materials that have been largely unexplored. We believe this type of material will have great potential application in chiral separations and enantioselective catalysis.

Experimental Section

Synthesis of **1a** and **1b**: A mixture of $CuCl_2\cdot 2H_2O$ (34.2 mg, 0.2 mmol) and 3-amino-5-carboxylic-1,2,4-triazole (26.4 mg, 0.2 mmol) in H_2O (5 mL) was sealed in a 25 mL Teflon-lined autoclave at 160 °C for 4 d, and then cooled to room temperature. Yellow block crystals of **1a** were recovered by filtration and air-dried (0.018 g, yield: 68% based on Cu). Elemental analysis calcd (%) for $Cu_{12}N_{24}C_{16}H_{32}O_8Cl_4$ (**1a**): C 12.06, N 21.10, H 2.01; found: C 12.01, N 21.12, H 1.99. IR (KBr): $\tilde{\nu} = 3300$(s), 2340(w), 1610(m), 1499(w), 1282(s), 1162(s) 1057(w), 924(w), 722 cm^{-1} (w). Compound **1b** was obtained by exposure **1a** in atmosphere for several weeks. Elemental analysis calcd (%) for $Cu_{12}N_{24}C_{16}H_{32}O_{14}Cl_4$ (**1b**): C 11.37, N 19.91, H 1.90; found: C 11.32, N 19.94, H 1.96. IR (KBr): $\tilde{\nu} = 3303$(s), 2340(m), 1627(m), 1499(s), 1284(s), 1163(s) 1055(s), 924(w), 722 cm^{-1} (w).

Received: August 6, 2010
Revised: September 28, 2010
Published online: November 29, 2010

Keywords: chirality · metal–organic frameworks · nanotubes · porous materials · single-crystal-to-single-crystal

[1] S. Iijima, *Nature* **1991**, *354*, 56.
[2] W. Tremel, *Angew. Chem.* **1999**, *111*, 2311; *Angew. Chem. Int. Ed.* **1999**, *38*, 2175.

[3] M. R. Ghadiri, J. R. Granja, R. A. Milligan, D. E. McRee, N. Khazanovich, *Nature* **1993**, *366*, 324.
[4] D. T. Bong, T. D. Clark, J. R. Granja, M. R. Ghadiri, *Angew. Chem.* **2001**, *113*, 1016; *Angew. Chem. Int. Ed.* **2001**, *40*, 988.
[5] S. J. Dalgarno, G. W. V. Cave, J. L. Atwood, *Angew. Chem.* **2006**, *118*, 584; *Angew. Chem. Int. Ed.* **2006**, *45*, 570.
[6] J. W. Mintmire, C. T. White, *Phys. Rev. Lett.* **1998**, *81*, 2506.
[7] T. D. Power, A. I. Skoulidas, D. S. Sholl, *J. Am. Chem. Soc.* **2002**, *124*, 1858.
[8] K. Huang, J. Rzayev, *J. Am. Chem. Soc.* **2009**, *131*, 6880.
[9] C. Piguet, G. Bernardinelli, G. Hopfgartner, *Chem. Rev.* **1997**, *97*, 2005.
[10] M. Albrecht, *Chem. Rev.* **2001**, *101*, 3457.
[11] S. N. Wang, H. Xing, Y. Z. Li, J. F. Bai, M. Scheer, Y. Pan, X. Z. You, *Chem. Commun.* **2007**, 2293.
[12] S. Q. Zang, Y. Su, C. Y. Duan, Y. Z. Li, H. Z. Zhu, Q. J. Meng, *Chem. Commun.* **2006**, 4997.
[13] Y. Cui, S. J. Lee, W. B. Lin, *J. Am. Chem. Soc.* **2003**, *125*, 6014.
[14] X. R. Hao, X. L. Wang, C. Qin, Z. M. Su, E. B. Wang, Y. Q. Lan, K. Z. Shao, *Chem. Commun.* **2007**, 4620.
[15] P. Vaqueiro, M. L. Romero, B. C. Rowan, B. S. Richards, *Chem. Eur. J.* **2010**, *16*, 4462.
[16] Y. Q. Sun, J. Zhang, Y. M. Chen, G. Y. Yang, *Angew. Chem.* **2005**, *117*, 5964; *Angew. Chem. Int. Ed.* **2005**, *44*, 5814.
[17] G. W. Orr, L. J. Barbour, J. L. Atwood, *Science* **1999**, *285*, 1049.
[18] E. Y. Lee, M. P. Suh, *Angew. Chem.* **2004**, *116*, 2858; *Angew. Chem. Int. Ed.* **2004**, *43*, 2798.
[19] K. Biradha, M. Fujita, *Angew. Chem.* **2002**, *114*, 3542; *Angew. Chem. Int. Ed.* **2002**, *41*, 3392.
[20] K. Biradha, Y. Hongo, M. Fujita, *Angew. Chem.* **2002**, *114*, 3545; *Angew. Chem. Int. Ed.* **2002**, *41*, 3395.
[21] H. R. Moon, J. H. Kim, M. P. Suh, *Angew. Chem.* **2005**, *117*, 1287; *Angew. Chem. Int. Ed.* **2005**, *44*, 1261.
[22] M. P. Suh, H. R. Moon, E. Y. Lee, S. Y. Jang, *J. Am. Chem. Soc.* **2006**, *128*, 4710.
[23] See Supporting Information for crystallographic details.
[24] X. L. Wang, C. Qin, E. B. Wang, L. Xu, Z. M. Su, C. W. Hu, *Angew. Chem.* **2004**, *116*, 5146; *Angew. Chem. Int. Ed.* **2004**, *43*, 5036.
[25] B. F. Abrahams, P. A. Jackson, R. Robson, *Angew. Chem.* **1998**, *110*, 2801; *Angew. Chem. Int. Ed.* **1998**, *37*, 2656.
[26] S. C. Chen, J. Zhang, R. M. Yu, X. Y. Wu, Y. M. Xie, F. Wang, C. Z. Lu, *Chem. Commun.* **2010**, *46*, 1449.
[27] R. E. Morris, X. H. Bu, *Nat. Chem.* **2010**, *2*, 353.
[28] B. Balamurugan, B. R. Mehta, S. M. Shivaprasad, *Appl. Phys. Lett.* **2001**, *79*, 3176.
[29] G. Férey, *Chem. Soc. Rev.* **2008**, *37*, 191.
[30] A. Demessence, J. R. Long, *Chem. Eur. J.* **2010**, *16*, 5902.
[31] C. Serre, C. Mellot-Draznieks, S. Surble, N. Audebrand, Y. Filinchuk, G. Férey, *Science* **2007**, *315*, 1828.
[32] A. L. Spek, *PLATON, A Multipurpose Crystallographic Tool*. (Utrecht University, Nethlerlands, **2001**).
[33] D. Saha, Z. B. Bao, F. Jia, S. G. Deng, *Environ. Sci. Technol.* **2010**, *44*, 1820.

